Venus Express observations of atmospheric oxygen escape during the passage of several coronal mass ejections

J. G. Luhmann,[1] A. Fedorov,[2] S. Barabash,[3] E. Carlsson,[3] Y. Futaana,[3] T. L. Zhang,[4] C. T. Russell,[5] J. G. Lyon,[6] S. A. Ledvina,[1] and D. A. Brain[1]

Received 29 January 2008; revised 21 April 2008; accepted 27 May 2008; published 26 August 2008.

[1] The solar wind interaction contributes to the loss of Venus atmospheric constituents, especially oxygen, by direct antisunward acceleration of planetary ions and possibly by related sputtering of neutrals. Both comet-like "ion pickup" and related sputtering processes may have played a key role in Venus' atmosphere evolution, but the significance of their effects, as well as other proposed escape mechanisms, is still uncertain. In particular, recent reports of only modest ion escape rates measured on Venus Express (VEX) during the current low-activity phase of the solar cycle make it important to reconsider the evidence seen in both Pioneer Venus Orbiter and VEX observations suggesting significantly enhanced escaping O^+ ion fluxes during periods of disturbed interplanetary conditions. At present, the most extreme interplanetary conditions result from the effects of coronal mass ejections (CME), which may have been more prevalent in the first 1–2 billion years of the Sun's history. The Analyser of Space Plasmas and Energetic Atoms 4 (ASPERA-4) Ion Mass Analyzer and Magnetometer on Venus Express have now made detailed measurements during several periods when CME disturbances encountered Venus. The observations and models described in this report provide further insights into the possible response of oxygen ion escape to solar activity. In particular, they illustrate nuances of in situ sampling of large-gyroradius pickup ions, related to the atmospheric source properties, spacecraft orbit geometry, and the prevailing interplanetary conditions, that make the estimation of the variable global escape fluxes due to that process particularly challenging. In three of the four cases examined in some detail, ionospheric oxygen ions were either unobservable or below the limit of detectability for passes well within interplanetary coronal mass ejection (ICME) intervals. In the fourth example, where ionospheric ions were observed as expected from the model, O^+ pickup ions were observed in greater abundance than is typical in undisturbed solar wind. Other escape processes are not considered here, although it is assumed the source population for the modeled pickup ions is a preaccelerated upper atmosphere component. Analysis of many more ICME events, expected to be obtained as the Sun becomes more active in future years, are necessary to resolve the question of the importance of ICME to Venus oxygen escape.

Citation: Luhmann, J. G., A. Fedorov, S. Barabash, E. Carlsson, Y. Futaana, T. L. Zhang, C. T. Russell, J. G. Lyon, S. A. Ledvina, and D. A. Brain (2008), Venus Express observations of atmospheric oxygen escape during the passage of several coronal mass ejections, *J. Geophys. Res.*, *113*, E00B04, doi:10.1029/2008JE003092.

1. Introduction

[2] One of the key planetary science issues for Venus (and Mars) is the evolutionary importance of the solar wind interaction [e.g., *Chassefiere*, 1997; *Lammer et al.*, 2006]. Our current picture of planetary atmospheric ion scavenging by direct interaction of the solar wind with weakly magnetized planets was developed in large part from observations obtained by the Pioneer Venus Orbiter, PVO [e.g., *Moore et al.*, 1990; *Brace et al.*, 1995], although the Venera mission first detected Venus' planetary ion wake [e.g., *Vaisberg et al.*, 1995]. The observations confirmed the presence of a comet-like interaction where the convection electric field of the solar wind, E = −VXB (where V and B are the bulk

[1]Space Sciences Laboratory, University of California, Berkeley, California, USA.
[2]Centre d'Etude Spatiale des Rayonnements, Toulouse, France.
[3]Swedish Institute of Space Physics, Kiruna, Sweden.
[4]Space Research Institute, Austrian Academy of Sciences, Graz, Austria.
[5]Institute of Geophysics and Planetary Physics, University of California, Los Angeles, California, USA.
[6]Department of Physics and Astronomy, Dartmouth College, Hanover, New Hampshire, USA.

0148-0227/08/2008JE003092$09.00

velocity of the solar wind and the interplanetary magnetic field vector, respectively) accelerates or "picks up" planetary ions near and above the exobase (~200 km altitude).The ions that become pickup ions may be either transported into the acceleration region by other forces such as those associated with pressure gradients, or they may be produced in situ from the local neutral gases. If they are accelerated to at least the ~11 km/s escape velocity for Venus, and are on outward trajectories that do not reimpact the exobase [e.g., *Luhmann and Kozyra*, 1991], they can be permanently lost. Other mechanisms for Venus ion escape have also been suggested that generally fall under the headings of 'ionospheric ion outflow' [e.g., *Barabash et al.*, 2007a] or 'bulk ionospheric escape' [e.g., *Terada et al.*, 2002]. However, many of the PVO observations at both high (~ keV) and low (~10s of eV) ion energies can be modeled by assuming that the pickup process dominates [*Luhmann et al.*, 2006, 2007] we focus on that process in the present analysis.

[3] It was also inferred from PVO measurements of both the upper atmosphere (observed by UV remote sensing and by the Orbiter Neutral Mass Spectrometer), the ionosphere (observed by the retarding potential analyzer, thermal ion mass spectrometer, and Langmuir Probe), and the ion fluxes moving antisunward in the nightside wake (observed by the Plasma Analyzer and Neutral Mass Spectrometer in its ion mode), that singly ionized atomic and molecular oxygen ions are the primary species involved in the solar wind-induced escape of the Venus upper atmosphere [e.g., *Brace et al.*, 1987, 1995; *Mihalov et al.*, 1995]. This is a consequence of the ion chemistry of a CO_2 atmosphere, where oxygen forms the bulk of the upper atmosphere and ionosphere [e.g., *Fox and Kliore*, 1997].

[4] Typical escape rates of oxygen ions from Venus today are low from an atmospheric evolution standpoint, little more than the equivalent of a weak cometary ion tail at approximately $10^{24}-10^{26}$ O^+ s^{-1} [e.g., *Moore et al.*, 1991; *Barabash et al.*, 2007a]. However, the Venus solar wind interaction represents one of the only ways to accelerate oxygen and other heavy atmospheric elements to escape speeds. The need for an effective loss mechanism for Venus oxygen has lately become a matter of special importance as arguments mount for a possible early ocean [e.g., *Grinspoon and Bullock*, 2007; *Kulikov et al.*, 2006]. One key question is whether this solar wind-enabled escape mechanism could have been sufficient, or whether instead, important quantities are sequestered and buried in oxidized regolith. This question bears on the expectations for future surface and subsurface mineralogy measurements at Venus in pursuit of a history of water on the planet. The broader consequences relate to general unmagnetized and weakly magnetized planetary bodies and satellites with atmospheres that interact directly with surrounding magnetized external plasma flows of any origin.

[5] *Luhmann et al.* [2006, 2007] revisited the PVO escaping O^+ ion observations to investigate the possible impact of disturbed solar wind plasma and interplanetary magnetic field conditions on escaping ion fluxes. The observations used in that study consisted of > 36 eV O^+ ion fluxes (~10 eV is required for O^+ escape from Venus) measured by the Orbiter Neutral Mass Spectrometer in its ion detection mode. The results suggested that enhanced incident solar wind dynamic pressures and interplanetary magnetic fields, such as those that occur during passage of interplanetary coronal mass ejections (ICME) and solar wind stream interaction regions are sometimes followed by detection of enhanced (by ~100×) escaping O^+ fluxes. What could not be determined from PVO measurements owing to the limited instrument capabilities, and orbital and temporal sampling coverage, is both the full range of the escape fluxes and the definitive escaping ion composition. In particular, evaluation of the escape flux requires knowledge of the details of its spatial and temporal variations, which are difficult to obtain with in situ measurements, while the composition measurements require ion mass spectrometry over an energy range from ~10 eV to > several 10s of keV.

[6] While several statistical analyses carried out on the PVO data revealed general patterns of the inferred O^+ escape flux spatial distribution, and average values of the fluxes along the spacecraft orbit [e.g., *Mihalov and Barnes*, 1982; *Moore et al.*, 1990; *Luhmann et al.*, 2006], it is not possible to reconstruct from these the global response to relatively rare and/or short-lived extremes in the solar and interplanetary conditions. Observation-validated models that allow the interpretation of global loss rates from local measurements provide the best alternative. In addition, the ASPERA-4 Ion Mass Analyzer, IMA, on Venus Express-VEX [*Barabash et al.*, 2007b] now routinely measures escaping O^+ fluxes with definitive mass identification in an energy range (0.01–30. keV) exceeding that available on PVO (e.g., see the discussion by *Luhmann et al.* [2006]). Since its orbit insertion in April 2006, Venus Express has witnessed a number of significant solar events [e.g., *Futaana et al.*, 2007], providing an excellent opportunity to investigate, with the supporting VEX magnetometer observations [*Zhang et al.*, 2006], the response of the escaping ions.

[7] The motivation for the study described here is to further constrain present rates of oxygen ion escape during ICME passages, toward evaluating the evolutionary importance of these conditions for Venus. VEX ASPERA-4 IMA and magnetometer observations are used, together with an MHD field-based test particle model of O^+ pickup ions, to analyze the escaping ion response during several events. The results illustrate that making the case for increased loss rates at these times depends critically on our ability to use models to interpret the observations. However, the observations reported here are independent of the assumption of any particular process and are of interest in themselves. Truly definitive results on the ion escape response will depend on the analysis of data obtained during a large number of different ICME as well as case studies. This will require measurements over at least one solar maximum period, the next of which will be underway in 2010–2012, together with models that take into account whatever processes are found to be significant.

2. ICME Observations on VEX

[8] Details of the VEX instruments used in this study can be found in papers by *Barabash et al.* [2007b] and *Zhang et al.* [2006]. The magnetometer is a dual triaxial fluxgate magnetometer where one triad is used to correct the

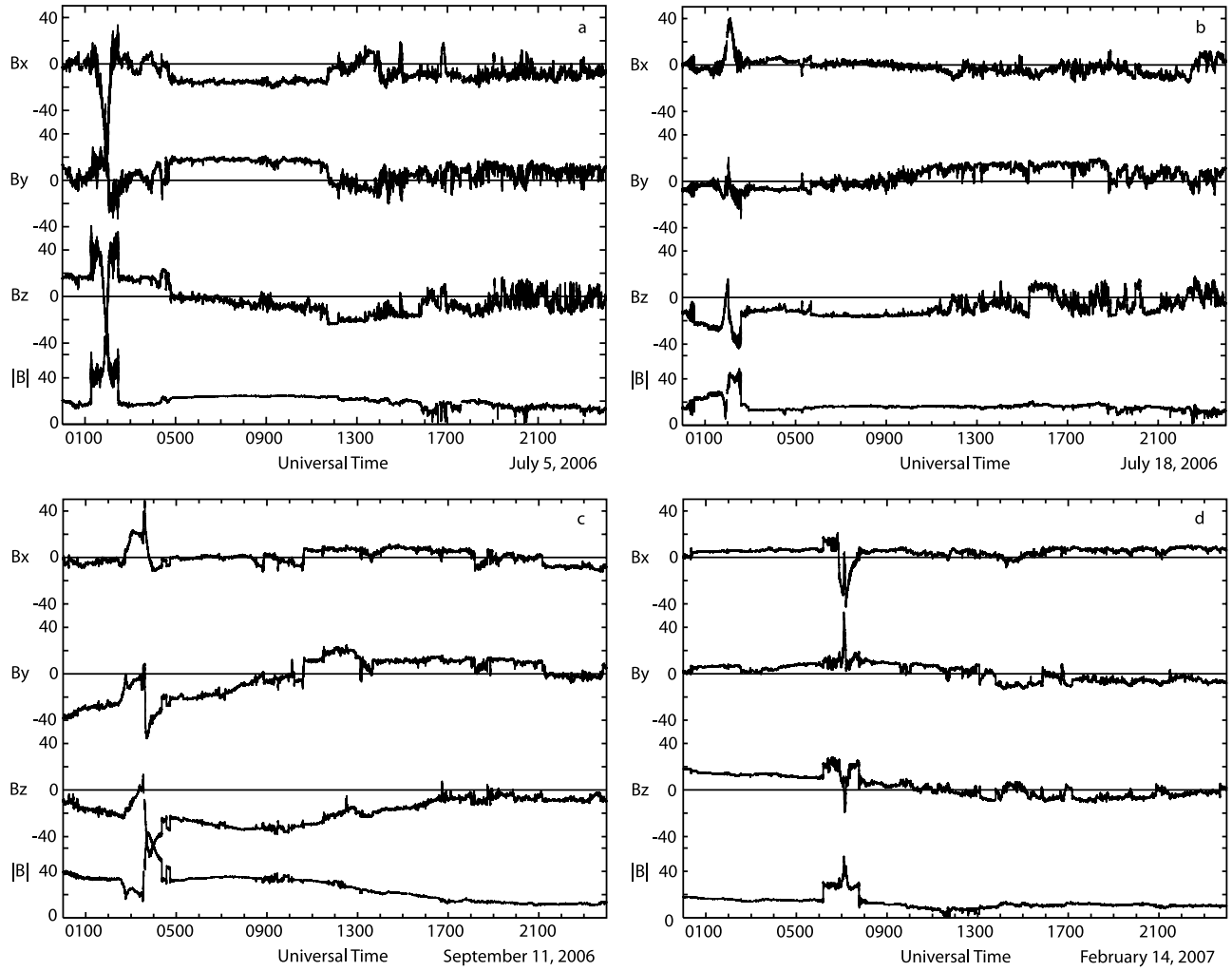

Figure 1. A set of four single orbit VEX magnetic field time series showing the ICME cases used here: (a) 5 July 2006, (b) 18 July 2006, (c) 11 September 2006, and (d) 14 February 2007. Near the beginning of each time series Venus perturbation is seen, including the bow shock, magnetosheath, dayside magnetic barrier, and magnetotail as sampled by VEX. The ICME field components exhibit an initial interplanetary shock and field pileup in the ICME sheath, followed by the smoothly rotating, often enhanced, solar ejecta fields sometimes lasting a day or more, although the start of the ICME is not always visible in these plots.

measurements for the spacecraft-generated magnetic fields [*Zhang et al.*, 2006]. The ASPERA-4 instrument is a close copy of the ASPERA-3 instrument on Mars Express [*Barabash et al.*, 2006], and includes both the ion mass spectrometer, called the IMA for ion mass analyzer, and an electron spectrometer, although here we concentrate on the data from the former. The mass range of the IMA is from 1 to 60 amu and the energy range is from 10 eV to 30 keV. The angular response of the IMA, which includes a deflection system, allows detection of ions coming from all azimuthal directions with respect to the Venus-Sun line, and from elevation angles of ±45°. Although the IMA is also a capable solar wind ion analyzer, ASPERA-4 operates only around periapsis to conserve instrument resources and to stay within its telemetry allotment (although there are occasional special full-orbit operations). Additional details of the IMA characteristics and operations are given by *Fedorov et al.* [2006] and *Barabash et al.* [2007b].

[9] VEX orbits Venus in a high-inclination elliptical orbit with ∼250–300 km periapsis close to the north pole [*Svedhem et al.*, 2007]. While the plasma analyzer operates only around periapsis, the magnetometer makes continuous measurements. To identify occurrences of ICME events in the VEX data we visually scanned magnetometer vector time series from 2006 and 2007 for the typical field signatures of ICME. These often include a leading shock jump and sheath (compressed solar wind) region, followed by larger than average, low-variance, smoothly rotating ejecta or driver fields. Typical duration of the entire disturbance is 1–2 days. Examples found in the PVO data at 0.73 AU are described in earlier papers by *Lindsay et al.* [1995], *Mulligan et al.* [1998] and in a recent paper by *Jian et al.* [2008]. The same signatures are used to identify ICME near the Earth [e.g., *Jian et al.*, 2006].

[10] Most unambiguous ICME events found in the VEX data occurred in 2006, when the Sun was more active. From

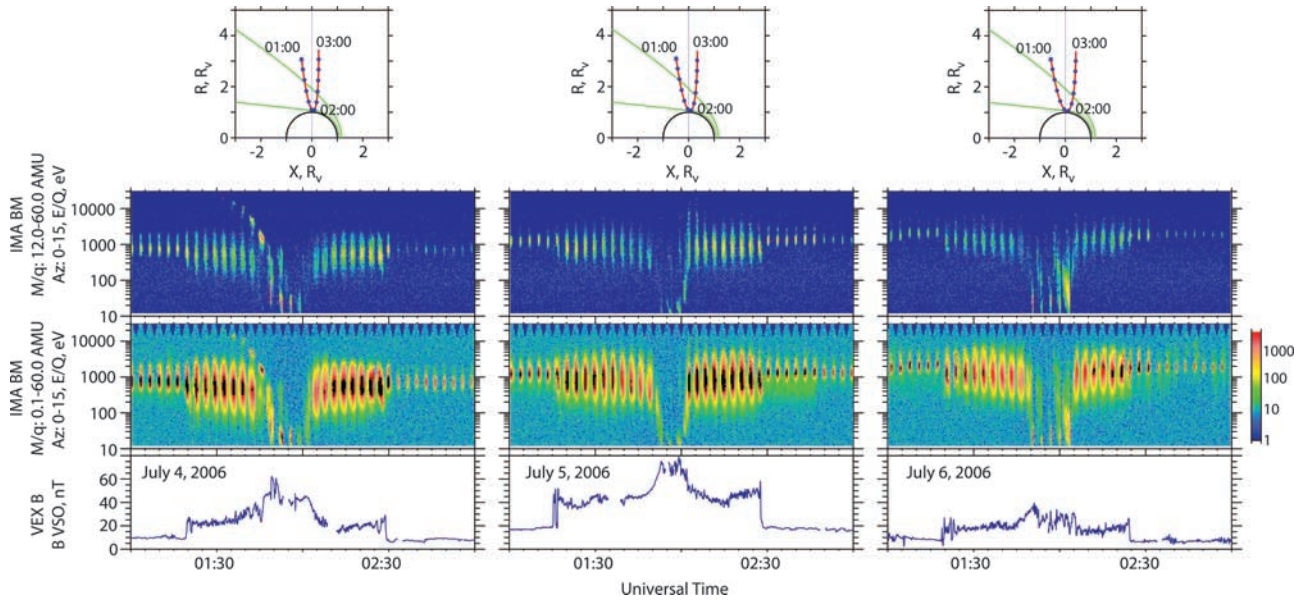

Figure 2a. Case 1: 5 July 2006 ICME ASPERA-4 IMA observations, together with the preceding and following orbits (days). The top panels show a 2-h orbit segment for these data, near periapsis. The top energy-time spectrograms include ions with masses 12–60 amu, while the bottom spectrograms include all ions detected. The latter is dominated by solar wind H^+. The bottom panels show the magnetic field magnitude from the magnetometer for context.

these, three cases were selected for detailed analysis because they exhibit the smooth, slowly rotating ejecta fields useful for analyzing and modeling the effects of the ICME conditions on pickup ions. A single case from 2007 was also included. In addition to the large, smooth ejecta fields, high dynamic and thermal pressures are found in the preceding postshock sheath of an ICME due to the ejecta's high velocity, solar wind density compression ahead of the fast-moving ejecta, and shock heating of the sheath solar wind plasma. However, these sheath periods last only a fraction of a day and so it is difficult to capture the Venus interaction at the VEX periapsis during the times of their passage. However, the high bulk speeds, and related high-convection electric fields and enhanced solar wind pressures, can persist throughout the passage of the ejecta, although they have typical solar wind densities. These attributes are not easily distinguished in the perturbed planetary interaction environment that ASPERA-4 samples near the VEX periapses, but their presence can still be inferred from the intervals of IMA data obtained outside the

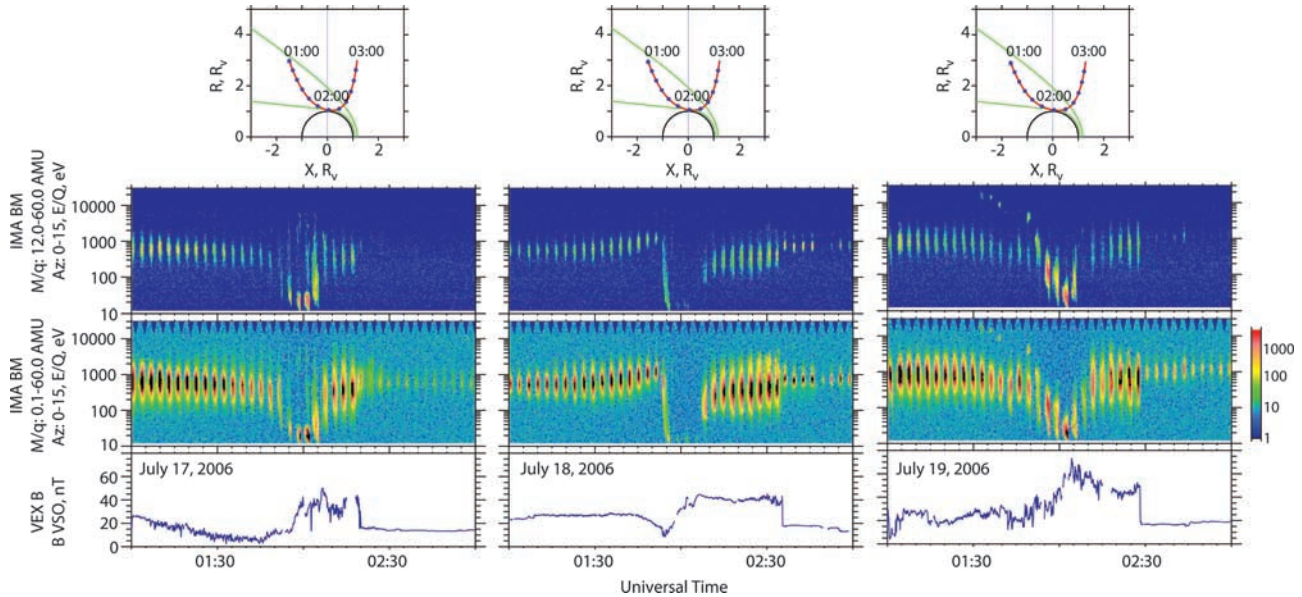

Figure 2b. Case 2: Same as Figure 2a but for the 18 July 2006 ICME.

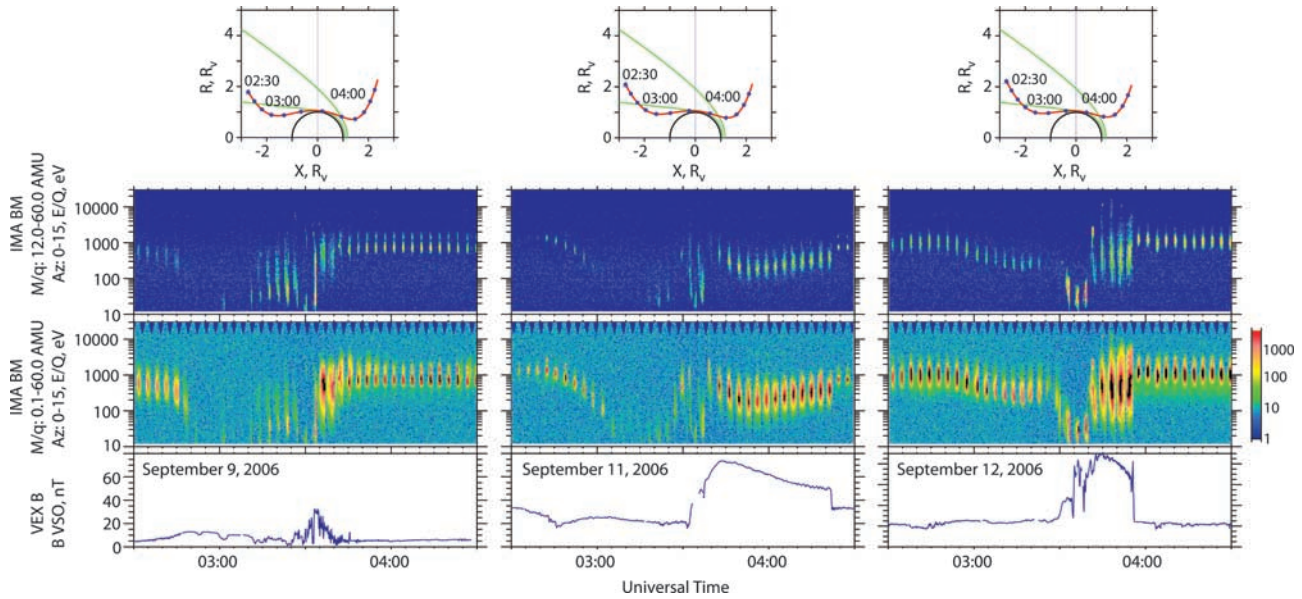

Figure 2c. Case 3: Same as Figure 2b but for the 11 September 2006 ICME. (In this case the pass in the first panel is a day earlier because ASPERA-4 data were not available the day before this ICME).

bow shocks. In the cases of the four ICME events analyzed here, the plasma velocities outside of the Venus bow shock were not especially high, an attribute not surprising for events occurring near solar minimum. Thus the main feature of these particular ICME is their steadier and larger than normal (by ~2x) interplanetary magnetic fields lasting a day or more, plus the expected (but not observed) shorter period of enhanced dynamic pressure from the preceding sheath higher densities.

[11] What are the possible consequences of ICME passage expected for Venus? In addition to a reduced ionopause altitude and ionospheric magnetization in response to the increased solar wind pressures in the ICME sheath [e.g., *Luhmann and Cravens*, 1991], ICME conditions are known to produce the largest convection electric fields and interplanetary field magnitudes detected in the interplanetary medium at 0.73 AU [e.g., *Lindsay et al.*, 1995]. Thus any processes affected by the convection electric field or ionospheric magnetization should be enhanced. In addition, the interplanetary shock-heated solar wind is expected to result in higher than usual Venus sheath electron temperatures and related impact ionization of any neutrals exposed to them, while the increased solar wind plasma densities in the ICME sheath can increase the rate of charge exchange (creating both additional ionization of the neutral O and energetic neutral hydrogen atoms, ENAs). The slowly varying, un-

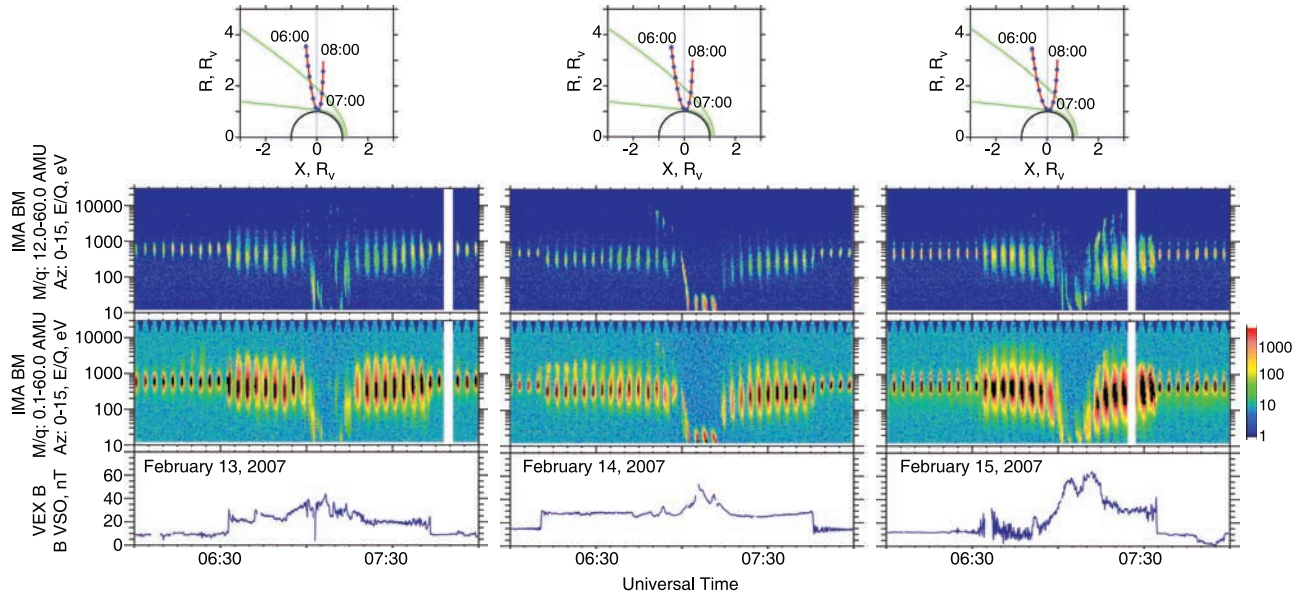

Figure 2d. Case 4: Same as Figure 2c but for the 14 February 2007 ICME.

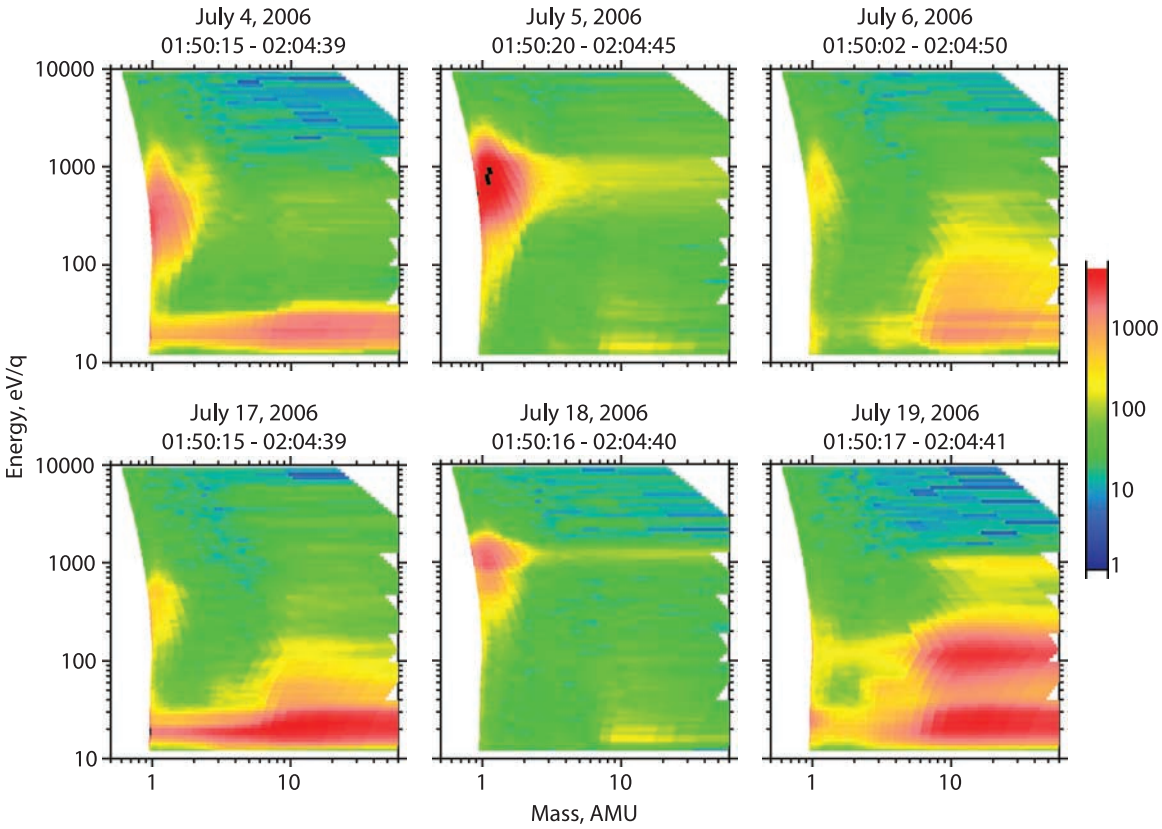

Figure 3a. ASPERA-4 IMA energy-mass diagrams for ICME cases 1 and 2. These show the ion composition for the 15 min around periapsis for the three passes (before, during, and after the ICME passage, from left to right), for (top) case 1 (Figure 2a) and (bottom) case 2 (Figure 2b). The heavy ions can be seen in the right part of the diagrams for the passes on either side of the central passes in Figures 2a and 2b. They consist mainly of O^+ and O_2^+, but heavier ions are also present.

usually steady magnetic fields of the ejecta meanwhile provide exceptionally simple conditions for analyzing and interpreting the behavior of observed ions in terms of the pickup process.

[12] Time series of VEX magnetometer vector components in the VSO system (x directed toward the Sun, y opposite the direction of planetary motion, and z northward from the Venus orbit plane) are shown in Figures 1a–1d for the days containing the selected passes. In all of these cases the ICME is already in progress when the day begins. The ICME are easily distinguished here by the previously mentioned low variance, slowly rotating ejecta fields, and by their field magnitudes, especially in the third example. For the first case shown, from 5 July 2006, the conditions surrounding the Venus interaction are dominated by high-inclination, northward (+Bz, clock angle 0) ejecta fields, while the 18 July 2006 case is dominated by high-inclination, southward (−Bz, clock angle 180) ejecta fields. The 11 September 2006 case has −By and −Bz (clock angle ∼225) dominated fields, while the 14 February 2007 case has +By and +Bz (clock angle ∼45) fields. Thus the selected cases provide a variety of external magnetic field orientations during ICME passages.

[13] ASPERA-4 IMA energy-time spectrograms for the four selected passes within the ICME events are shown in Figures 2a–2d, together with the total magnetic field and orbit near periapsis in the cylindrical view (where the y and z positions are converted into a cylindrical coordinate projected into a plane perpendicular to the Venus-Sun (x) axis). As controls, we also show the spectrograms for the adjacent periapsis passes the day before and the day after the main event passage. (The VEX orbital period is approximately an Earth day, also the approximate duration of a typical ICME.) The orbit segments at the top of each pass illustrate the spacecraft sampling in local time, solar zenith angle, and radius. The spectrograms are shown for both all detected ions (0–60 amu) and heavy (>12 amu) ions only. The total ion spectrograms are included to provide the solar wind plasma context of the measured heavy planetary ions. Note that the light ions may also include some picked-up planetary H^+, H_2^+ and He^+ ions [e.g., *Barabash et al.*, 2007a], but we exclude these from consideration in our present analysis focused on oxygen. The total ion spectrograms are dominated by the standard solar wind interaction features including proton heating at the bow shock (seen as broadening of the main solar wind proton band in the energy-time spectrogram), the compression and deceleration in front of the ionospheric obstacle, and the reduction or disappearance of solar wind proton densities in the wake. The periodic dropouts in the detected fluxes are a result of the directional sampling cycle of ASPERA-4 and the anisotropy of the detected ions, most of which flow approximately antisunward. Near-periapsis magnetic field magnitude time series are plotted at the bottom to provide

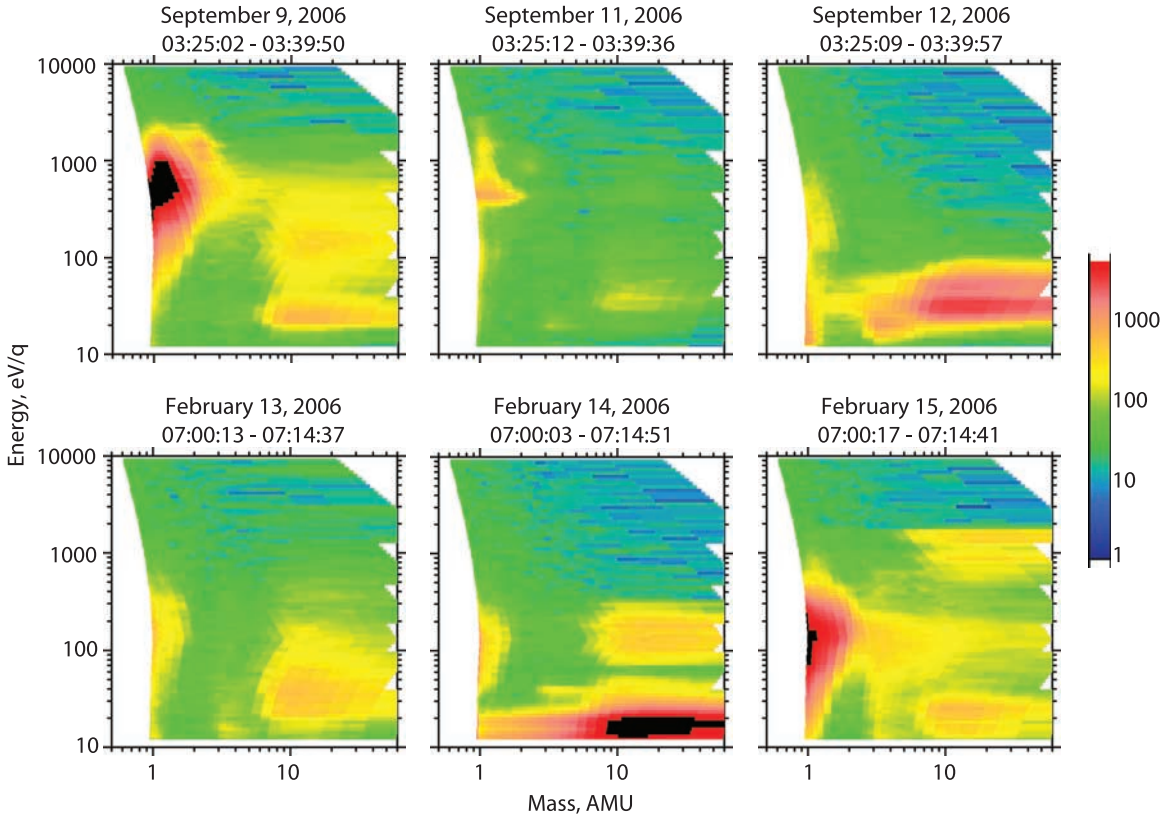

Figure 3b. Same as Figure 3a but for ICME cases 3 and 4 in Figures 2c and 2d. For case 3 (top row), the pre-ICME pass is two days ahead. For case 4 (bottom row) it is a day ahead. Case 4 is the only one of the four with high (saturated counts) oxygen ion content in the central diagram, during the main portion of the ICME passage.

a perspective on the location of the ion features relative to the magnetic pileup signatures in the sheath.

[14] The heavy ion spectrograms in the second panels from the top of each example in Figures 2a, 2b, 2c, and 2d are dominated by atomic oxygen, but may also contain contributions from O_2^+, CO^+, and CO_2^+ [*Carlsson et al.*, 2006]. As shown by the IMA mass-energy plots of *Barabash et al.* [2007b], these also include 'shadows' of the solar wind due to the high flux of protons and the resulting overlap in mass-energy space. The species separations used for the heavy ion spectrograms are obtained with Gaussian distribution fits to the overlapping mass peaks in the mass-energy plots [e.g., *Carlsson et al.*, 2006]. These spectrograms exhibit several distinctive features including a period dominated by lo—energy ions within the 10–20 min interval around periapsis (roughly the plot center), and a more energetic heavy ion signature with a highly variable appearance. The low-energy ions are typically in the 10eV to a few 10s of eV energy range, and are thus already at escape energies for oxygen. The latter may appear as a faint high-energy component during the same time period that the low-energy ions are observed, or it may be observed outside the periapsis interval in the adjacent magnetosheath, together with the solar wind protons. The magnetosheath cases closely resemble what was observed in the PVO plasma analyzer data in similar time-energy spectrograms without mass separation [e.g., *Luhmann et al.*, 2006]. In a few passes the energies of the heavy ions around periapsis appear to dip below the IMA energy threshold. A possible relationship between the low-energy and high-energy components will become apparent in the discussion of the modeling results below.

[15] The key observational result derived from these events is best seen with the help of mass-energy analyses of the data in Figures 2a–2d. Figures 3a and 3b show mass-energy plots obtained from the 15 min around periapsis for the four event passes and for passes before and after the main event pass. The color scale indicates the detector counting statistics for these samples, which are approximately proportional to the flux. It is seen that three of the four event passes show a near or total absence of counts at the heavy ion masses compared to the passes during relatively typical interplanetary conditions. The one exception out of the four, on 14 February 2007, in contrast shows an exceptionally high (saturated) count rate for the heavy ions in the same near-periapsis sample. The possible reasons for the nondetection of the mainly oxygen ions at these times for the other cases, both at periapsis and in the adjacent sheath, are best investigated with models of the global distribution of escaping ions.

3. Model Analysis of the VEX Ion Observations

[16] As noted in the introduction, we here assume that the pickup process describes the bulk of escaping heavy ions observed by the ASPERA IMA around Venus. This as-

sumption provides a starting point for analysis that has observational support from PVO results, and can also lead to insights on whether other processes are important.

[17] Venus pickup ions include all planetary ions that are accelerated by the action of the underlying convection electric field, whether they are escaping or on trajectories that return them to the atmosphere. It is important to appreciate that the pickup process is not restricted to the magnetosheath and solar wind outer regions. If the solar wind magnetic field penetrates the upper atmosphere between the ionopause and the exobase (or even below it), and a flow is present, an ion can still be accelerated by $E = -VXB$. Different processes may also combine. For example, some ions may first move in response to other forces such as pressure gradient forces, and then attain escape speed when they are transported into a region where the convection electric field leads to their further acceleration. It is also important to remember that, unless they are observed in the mid-to-distant wake, pickup ions detected along a spacecraft orbit do not necessarily contribute to an escape flux. In determining whether an observed O^+ ion is escaping or not, one must consider its energy, its location with respect to the planet, and its direction of motion. One also needs to know how representative the orbital sampling of the escaping ions is of the total escaping ion population. A global model of the ions is thus extremely useful for determining both whether a particular observed O^+ flux is escaping, and what the implications of the local measurements are for the overall loss rates.

[18] As also mentioned above, one of the striking features of the heavy ion spectrograms in Figures 2a–2d is their diverse appearances. Most show a period of enhanced fluxes around periapsis at the lowest energies and altitudes measured. These probably represent the pickup O^+ source region in the upper ionosphere that is dominated by ionization and nightward transport of the dayside thermosphere neutral O source, rather than by the much more rarefied exospheric O from dissociative recombination of ionospheric O_2^+. The coexistence of cold and hot oxygen atmospheric components in the pickup ions has been discussed previously (e.g., recently by *Luhmann et al.* [2007]). The ion spectrogram features at the higher altitudes exhibit the inbound-outbound asymmetries expected from the pickup process and the finite heavy ion gyroradius effects found for the more energetic pickup ions. When the interplanetary magnetic field component perpendicular to the solar wind velocity rotates from one angle (or clock angle) to another, the appearance of the pickup ion wake signature can change dramatically [e.g., *Kallio et al.*, 2006]. But we do not even know how the low- and higher-energy ion observations are related to one another, or if their variation on the global scale is coupled. Such key outstanding questions only emphasize the difficulty of inferring global ion escape rates from one or two orbits during special events such as ICME passages.

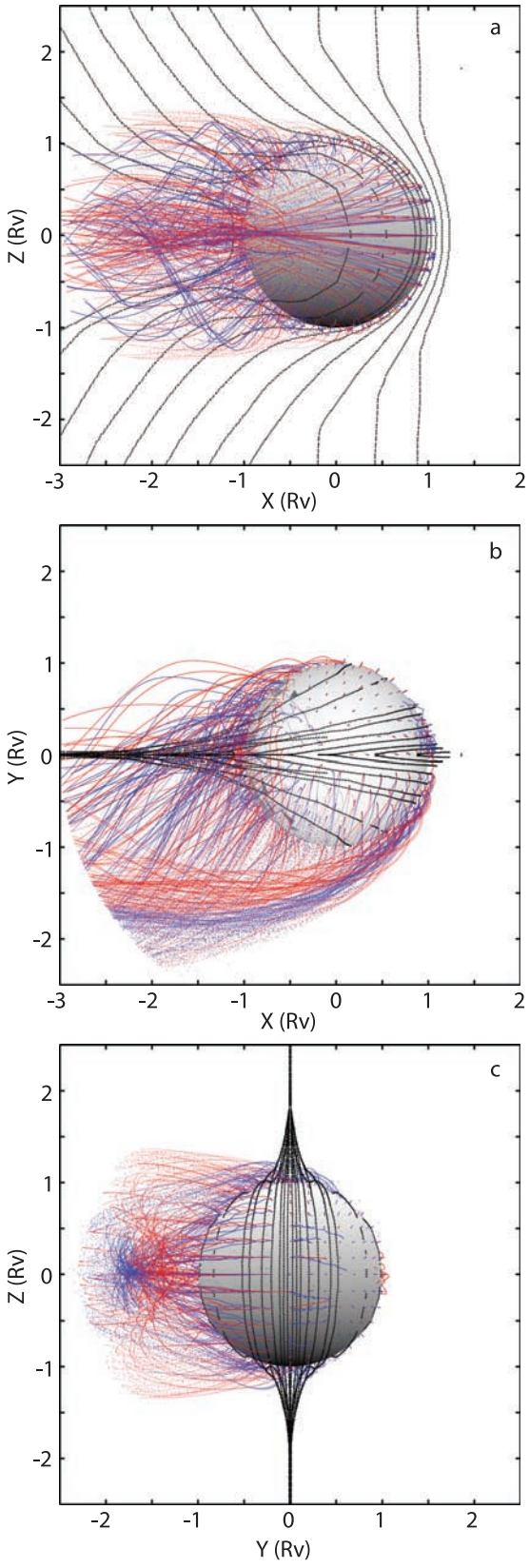

Figure 4. Orthogonal views of some MHD model field lines (black) with superposed test particle O^+ trajectories for MHD fields without (red) and with (blue) mass loading near the Venus obstacle. The model interplanetary field is northward (clock angle = 0). (a) Noon–midnight plane projection; (b) ecliptic plane projection; and (c) view from the Sun, looking tailward. The trajectories are traced to 3 Rv. These illustrate both the asymmetry and the spatial concentration of the oxygen pickup ion "wake."

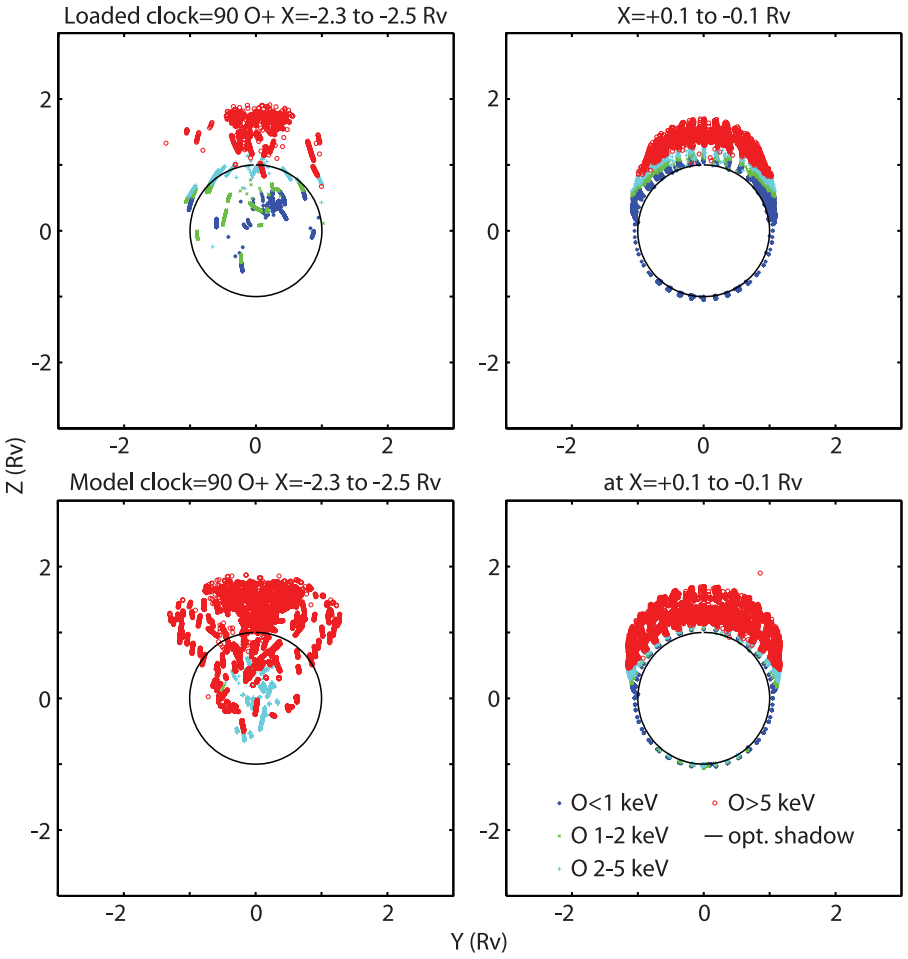

Figure 5. (top) Cross sections of the picked up O^+ ion wake at the (right) terminator plane and (left) down-tail color coded by ion energy. This case uses the MHD model with mass loading effects and is for 90° (+y) interplanetary field clock angle. The northward pointing convection electric field produces the north-south asymmetry. (bottom) Same as top but using the MHD fields and flows without mass loading effects.

[19] The model of the global pickup process that we use here has been validated by comparisons with magnetic fields measured on PVO [*Kallio et al.*, 1998], and with PVO plasma analyzer measurements of O^+ [*Luhmann et al.*, 2006]. The background fields and flows are provided by an MHD model of the typical 0.73 AU solar wind interacting with a spherical conductor whose radius is at the nominal subsolar ionopause height for Venus, with an interplanetary magnetic field perpendicular to the incident flow direction. The trajectories of planetary O^+ ions are traced as test particles in these background magnetic fields and flows. We use the same numerical equation of motion solver, including the Lorentz force and Venus gravity, as used by *Luhmann et al.* [2006]. The test particle pickup ions' properties (energy and directional distributions) are the collective result of the assumed distribution of O^+ starting points, their initial velocities, the geometry and strength of the background MHD model magnetic fields, and the bulk plasma flows that together with these magnetic fields describe the E = −VXB convection electric field. The effects of the Venus-Sun (x) component of the interplanetary magnetic field are not included in this model. This allows us to rotate the model results around the Venus-Sun or *x* axis to approximate the effects of orbital sampling of the pickup ion population for different interplanetary field clock angles (relative to Venus North). The x component of the field is known to introduce some dawn-dusk asymmetries into the plasma interaction with Venus and so its neglect should be kept in mind, but for many analyses this is a secondary effect.

[20] Two versions of the MHD model were used to calculate the pickup ion trajectories: one assumes the solar wind interacts with the conducting spherical obstacle with no effect of the production of heavy ions in the inner magnetosheath. Such a scenario might apply if the ionopause is at higher altitudes due to a low solar wind pressure or an enhanced ionospheric pressure. The other version assumes mass loading of the underlying flow by heavy O^+ ions consistent with a simplistic approximation to photoion production from both thermospheric and exospheric atomic oxygen above the dayside of the planetary obstacle. (See *Kallio et al.* [1998] for further details.)

[21] To illustrate the basic nature of the pickup ion spatial distributions and their sampling by the VEX orbit, Figure 4

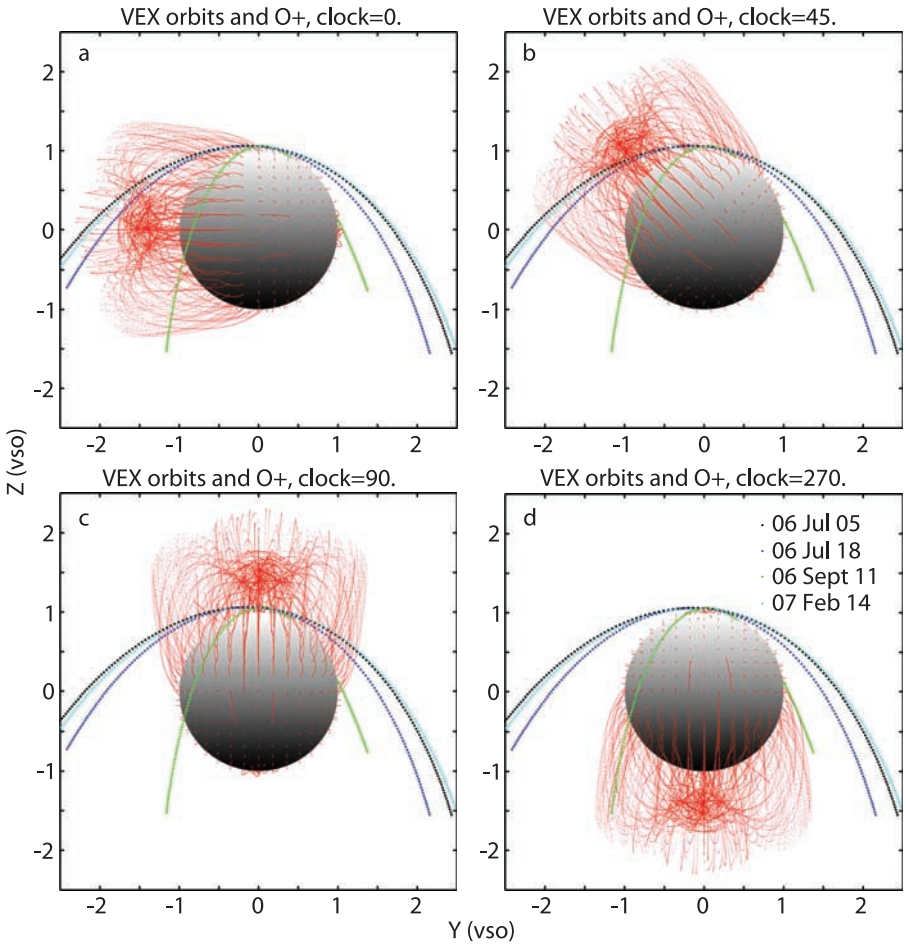

Figure 6. Illustration of VEX periapsis pass sampling of model O^+ trajectories (obtained with the MHD field and flow model with no mass loading) for four interplanetary field clock angles: (a) 0°; (b) 45°; (c) 90°; and (d) 270°. The view is from the Sun. These suggest how an in situ ion observer's perspective could be biased by a particular orbit's geometry of intersection with the ion wake.

compares the trajectories of several hundred O^+ ions launched on a spherical shell within a few hundredths of a planetary radius of the MHD model's inner boundary for MHD model fields with (blue) and without (red) mass loading. The trajectories are traced to 3 Rv (Rv = the Venus obstacle in the model (planet plus ionosphere) ~6300 km), a distance that covers the VEX orbit sampling of near-Venus space. Three projections, one as seen from the Sun, one in the ecliptic, and one in the noon–midnight plane are shown. The pickup ion distribution global asymmetry seen here, with the highest concentration of large-gyroradius trajectories initially moving toward the hemisphere where E = −VXB points, is a well known signature of the pickup process. While the two cases produce similar trajectories, the mass loaded case trajectories are more spatially concentrated when seen in cross section from the Sun. In both cases it is apparent that one's assessment of the escaping ion fluxes in such a distribution will depend on where and when they are sampled as the spacecraft orbits and the interplanetary field (and ion wake) rotate.

[22] Figure 5 displays complementary plots of the locations where the modeled pickup ions cross thin cross-sectional slabs at the terminator and downstream for the cases with (Figure 5a) and without (Figure 5b) mass loading. Here the interplanetary field is along the +*y* axis so that the maximum density of the asymmetric pickup ion wake seen in Figure 4 is in the north or +z half plane. The existence of a wedge-like feature and a low-energy central wake concentration at several Rv downstream is consistent with VEX results reported by *Barabash et al.* [2007a] from statistical analyses of the oxygen ions in the Venus wake, while the terminator cross section asymmetric bulge in the direction of the upstream convection electric field is consistent with reported ionopause cross section asymmetries seen on PVO [*Phillips et al.*, 1988]. These cross sections, together with the ion trajectories in Figure 4, emphasize the asymmetry and limited cross section of the pickup ion wake, properties that are critical when evaluating global escape rates from limited orbital sampling. This is further emphasized by Figures 6 and 7 which show the four selected periapsis orbit segments together with the pickup ion trajectories. The ion trajectories have been rotated to three orthogonal positions to represent the effect of a range of interplanetary field clock angles on the orbital sampling

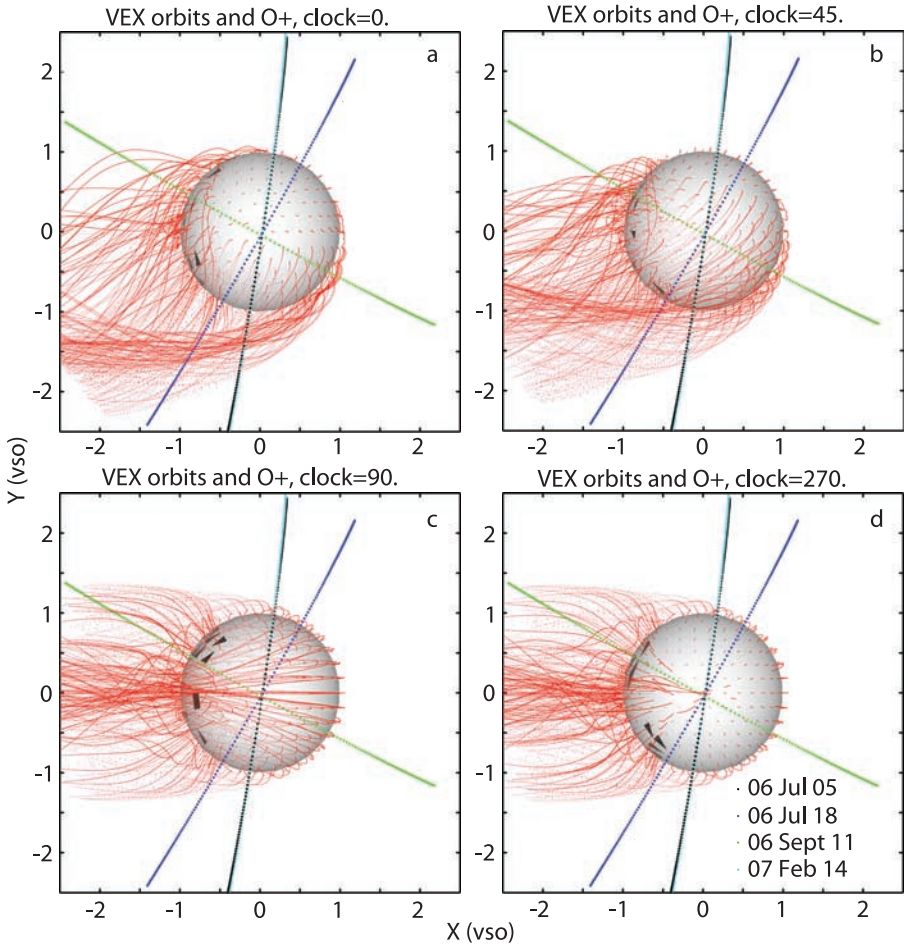

Figure 7. Same as Figure 6 but for the ecliptic plane projection: (a) 0°; (b) 45°; (c) 90°; and (d) 270°.

geometry. These illustrate that one could infer a large range of ion escape fluxes, from negligible to representative of the maximum, from what is measured along the same VEX orbit, depending on the location of the orbital plane and the prevailing interplanetary field. Models provide a way to better understand the implications of the observations and also allow numerical experiments to determine which model assumptions produce results consistent what is observed.

[23] To obtain the general character of the VEX heavy ion energy-time spectrograms, we found the following choices for the O^+ starting grid were necessary: (1) starting points only in a narrow altitude range near the inner (spherical) model boundary; (2) a starting point grid including both dayside and nightside hemispheres, rather than just the dayside; (3) nonzero test particle starting velocities. The first of these was necessary to reproduce the narrow (in energy) pickup ion signatures; the nightside grid was necessary to obtain the observed deep wake fluxes of O^+ near the base of the induced magnetotail current sheet separating the tail lobes; the nonzero starting velocities allowed the consistent reproduction, with the same model, of the low-altitude, low-energy ion signature and the sheath energetic ion signatures for the same pass. This last assumption also has the merit that PVO Retarding Potential Analyzer observations [*Miller and Whitten*, 1991] showed significant (~5–10 km/s, up to nearly 10 eV) antisunward thermal O^+ flows in the upper ionosphere at solar zenith angles near and beyond the terminator plane, interpreted to result from day-to-night ionospheric plasma pressure gradients.

[24] To illustrate the general characteristics of the modeling results we show in Figure 8 simulated O^+ energy-time spectrograms for eight interplanetary field clock angles, spaced at 45° intervals, for the trajectory associated with the 18 July 2006 periapsis. This pass provided a particularly good trajectory for illustrating the asymmetries in the pickup ion distribution because it roughly samples the northern hemisphere in the terminator plane from dawn to dusk. We found it was not necessary to use many ions or a closely specified altitude of the starting point grid to establish the general patterns in the spectrograms, thus we started approximately 1200 O^+ ions uniformly distributed over a spherical grid at 1.05 times the obstacle radius. The results are shown for two cases: the background MHD model without mass loading and an initial O^+ velocity of a few 10s of km/s at the terminator, and an MHD model with some rudimentary ionospheric mass loading (see discussion of these two models by *Kallio et al.* [1998]), and a lower (by 0.1x) initial O^+ velocity. The spectrograms were constructed by calculating the number of constant time step ion trajectory points falling within spherical volumes of 0.1 Rv radius, stepped along the VEX orbit through the

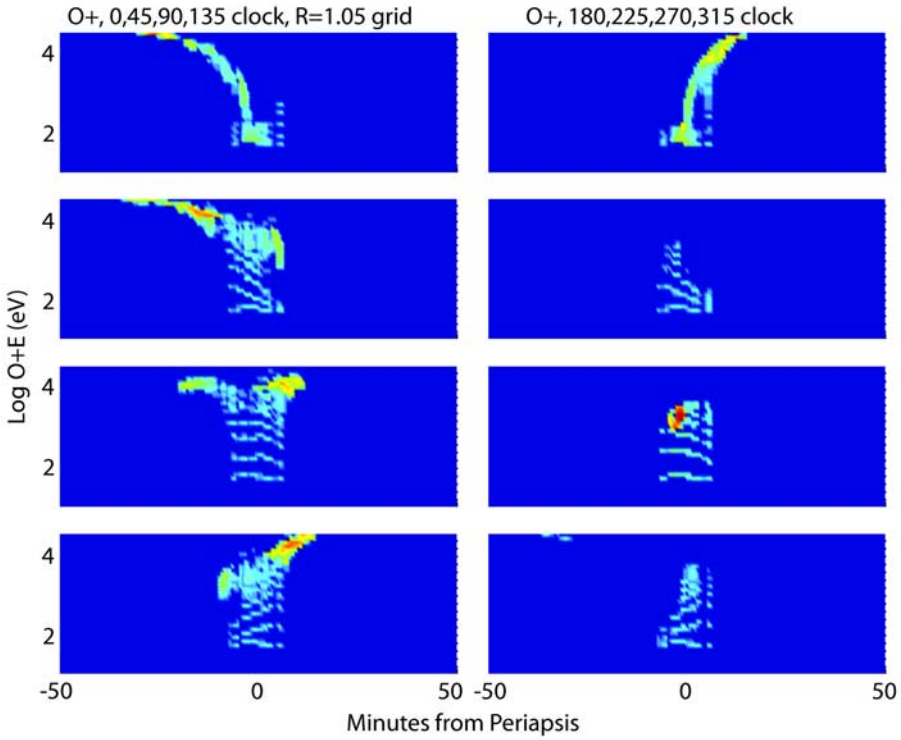

Figure 8. Simulated ASPERA-4 IMA O^+ spectrograms for the nominal (no mass loading) MHD field and flows case, for clock angles spaced 45° apart, obtained by "flying" the 18 July 2006 orbit through the modeled ion wake. As expected, the spectrograms look very different, although the ion wake is the same in all cases.

periapsis pass. The velocity vectors of the particles entering the spherical volumes were filtered to accept only those within the ±45° elevation angles accepted by the IMA. The color scale and its range are analogous to the log (counts) scale in the VEX spectrograms. Here the model statistics provide an idea of the numbers of O^+ trajectory points falling within the sampling spheres. These statistics are proportional to the IMA counts. As mentioned above, the assumption of the initial velocity of the ions affects the low-energy near-periapsis O^+ signatures, as does the use of mass loaded versus not loaded MHD field and flow models.

[25] The general patterns in the modeled heavy ion spectrograms in Figure 8 resemble those in the observations in Figures 2a–2d. In particular they reproduce the occasionally observed narrow bands of high intensity O^+ in the sheath on inbound and/or outbound legs with velocities (energies) that smoothly increase (decrease) as the spacecraft altitude increases (decreases). In the model, these features do not represent a time-dependent acceleration

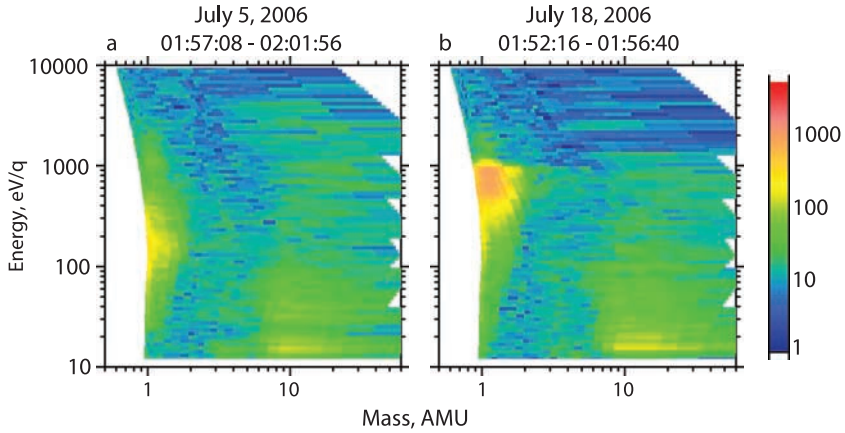

Figure 9. Energy-mass diagrams for the narrow layers (5 min duration) visible on (a) the outbound leg of case 1 and (b) the inbound leg of case 2 ICME pass spectrograms shown in the middle of Figures 2a and 2b. O^+ appears to be present in these features.

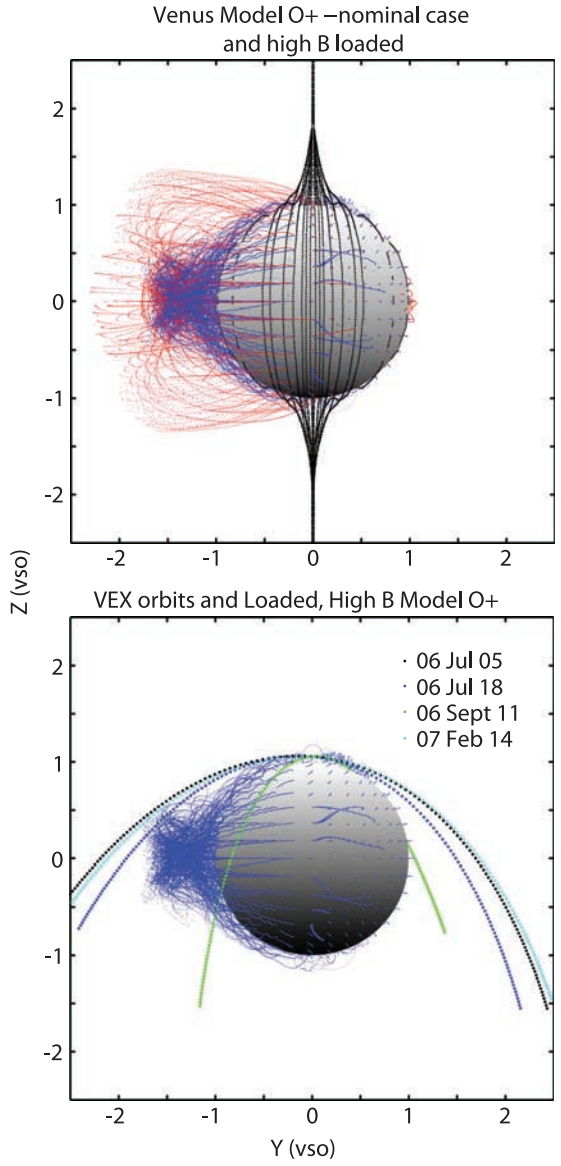

Figure 10. (top) Views from the Sun of the O^+ trajectories in the nominal model (red) and for a mass-loaded, increased (3×) interplanetary field model (blue). (bottom) VEX ICME orbit sampling of the latter model. The VEX orbit intersects much less of the pickup ion wake owing to the reduced O^+ gyroradius and the already confining effects of the mass loading on the O+ wake extent.

signature, but rather sampling of a stationary spatial distribution of ions, with locally narrow energy spectra at each location. They are analogous to the features referred to as beams in the literature [e.g., *Carlsson et al.*, 2006], although the ions are beam-like only in the sense that they have narrow energy spectra and are traveling in approximately the same directions at a given location. The term ring beam distribution, widely used in pickup ion studies, is the better descriptor.

[26] A key result is that for some clock angles practically no model pickup ions are detected along the VEX orbit even though the global pickup ion population, including the escaping component, is identical. In these cases the narrowness and low altitude of the production layer, coupled with the magnetic field clock angle, minimize the orbit's intersection with the pickup ion wake. Of special interest for the ICME observations are the spectrograms for 0° and 180° clock angles. One characteristic of ICME ejecta fields is rotation to large inclinations out of the ecliptic plane. The model results suggest that the prominent pickup ions features in the sheath should become observable as the ICME fields sweep through the large inclinations. However, the observations in Figures 2a–2d show that this is generally not the case during the periods of the selected ICME passes, which are short on the ICME timescales (compare Figure 1). The approximate clock angles at the times of the IMA data are ∼0° for the 2006 5 July case, ∼180° for the 2006 18 July case, ∼225° for 2006 11 September case, and ∼45° for 2007 14 February. Only in the last case does the VEX heavy ion spectrogram show the O^+ feature suggested by its model counterpart in Figure 8, although the orbital sampling differs from cases 2 and 3.

[27] These model results also assume fixed typical solar wind B and V magnitudes of about 14 nT and 400 km/s, respectively, while the ICME often have higher B by a factor of ∼2 or more, and higher V by up to a factor of ∼4. The combined higher V and B effects on the ion trajectories will offset one another somewhat because the gyroradius is proportional to particle v, which is accelerated to up to twice the ambient flow speed, and inversely proportional to B. However, the higher V means that the energies attained by the picked up O^+ can be much larger than is typical. Thus the O^+ trajectories can be the same but the O^+ energies may exceed the energy range of the ASPERA-4 IMA. In such cases the IMA would still observe the lower altitude, lower energy portions of the picked up O^+ features, and just not detect the full energy-dispersed features in the sheath. However, this does not seem to be the case in our first three examples. In addition, the solar wind velocities for the four selected ICME, obtained by inspection of the IMA energy-time spectrograms in Figures 2a–2d, seem to rule out an energy range limitation to the picked up O^+ detection in the sheath. For the pass on 5 July 2006 the center of the solar wind spectral band prior to and after the broadening due to the shock suggests a nominal solar wind proton energy only slightly greater (∼1.3 keV) than the typical 1 keV. In fact many ICME travel only modestly faster than the ambient solar wind. On 18 July 2006, only the outbound shock is visible in the spectrogram, but it too suggests solar wind proton energies at or slightly less than the typical 1 keV. The 11 September 2006 case also shows only outbound solar wind, again near 1 keV, and the ICME segment passing on 14 February 2007 appears to have only 800 eV solar wind protons. However, while none of the cases under consideration here should be subject to the IMA energy range upper limit mentioned above, we expect the strongest events to be affected in this way.

[28] A more likely explanation for the apparent absence of significant O^+ in the IMA spectrograms may be the increased magnetic fields. Figure 9 shows energy-mass analyses of the very narrow features inbound on 5 July 2006 and outbound on 18 July 2006, where the spacecraft apparently enters and leaves the ionosphere. These reveal that O^+ is indeed present for those short periods (∼5 min.). In addition, hints of O^+ below the 10 eV lower threshold of

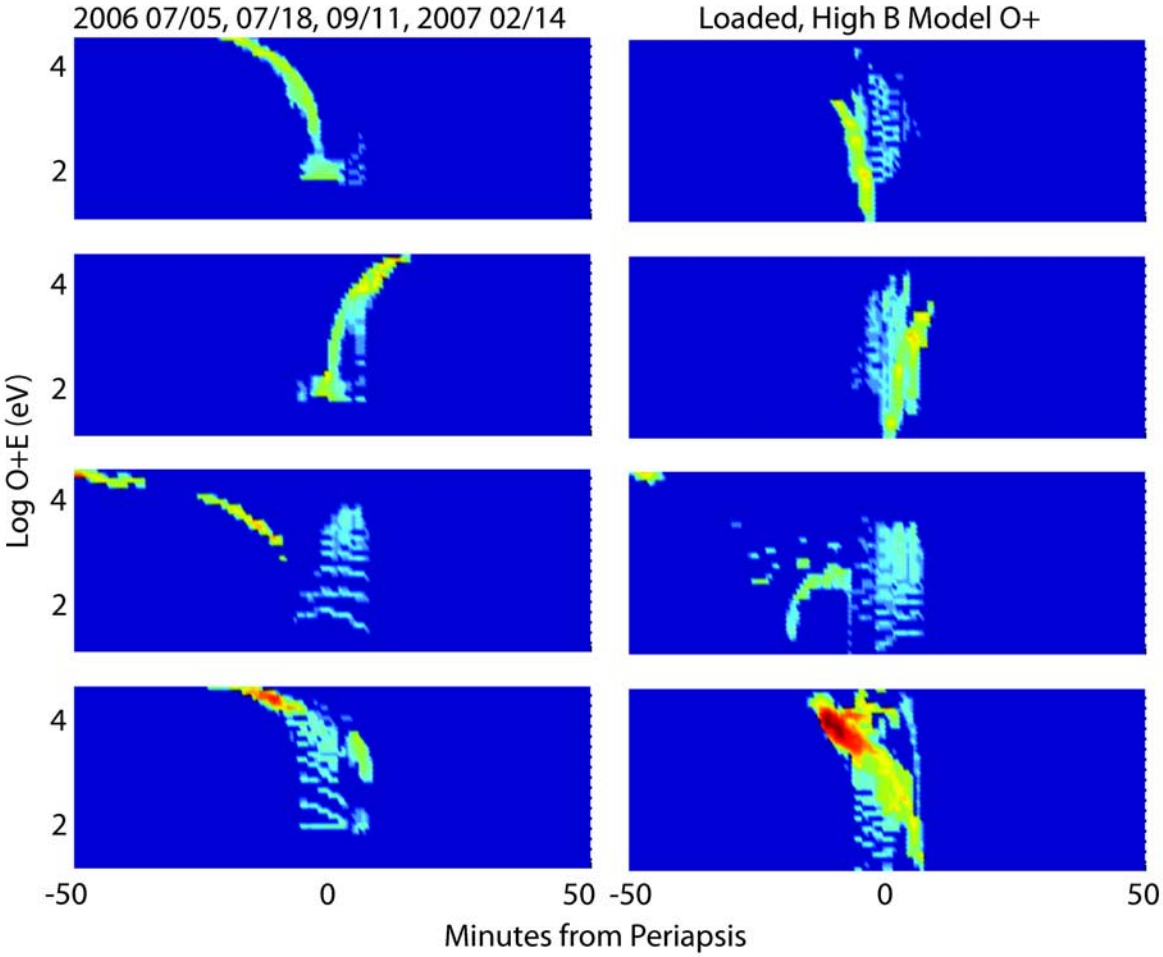

Figure 11. Simulated ASPERA-4 IMA O+ spectrograms for the four selected ICME. The left column is the nominal (not-loaded) model; the right is for loaded plus high field. The most striking features consistent with the observations in Figures 2a–2d are the energy-dispersed, spectrally narrow features occasionally seen in the sheath regions. The other notable features also present in the VEX data are the occasional low-energy ion enhancements observed throughout the lowest altitude portion of the pass. The origins of these features are discussed in the text.

the IMA energy range in both cases suggest that intensive mass loading of the solar wind interaction boundary at these times reduces the initial velocities of the source O^+. In addition, the larger magnetic field magnitudes during the ICME reduce the pickup ion gyroradii so that the pickup ion wake spatial distribution may be more closely confined to the optical wake. As an approximate model of these conditions we used the mass loaded MHD field and flow results with the magnetic field multiplied by 3×, and the lower O^+ starting velocities (~2 km/s) used for the mass-loaded case as described earlier. The particle trajectories for this case are compared with the nominal case and with the spacecraft near-periapsis trajectories in Figure 10. The larger magnetic field reduces the O^+ gyroradius as expected, altering the ion wake cross section and its orbital intersection. In Figure 11 the resulting O^+ spectrograms for the four ICME cases are compared with the same orbital samples of the normal (standard magnetic field, no mass loading) model for the event pass trajectories. The high field, mass loaded case on the right shows attributes that tend toward the observed ICME heavy ion spectrogram behavior: an absence of the long, energy-dispersed sheath ion features, and O^+ concentrated in nearly vertical features at the boundaries of the source region entry and exit. A feature that remains puzzling, and for which we have no explanation, is the apparent opposite sides of these latter features from what would be expected for the 5 July and 18 July 2006 cases with 0° and 180° clock angles respectively. Clearly there is a need for carrying out more specific simulations using the observed ICME external parameters, with a detailed treatment of the ionospheric source, in order to obtain more realistic background fields and with them, more accurate models of the picked up O^+ behavior.

4. Conclusion

[29] So is there any evidence that the ICME selected for study in this paper produced an increase in the escaping pickup O^+ fluxes? For the four selected events examined here, perhaps only in one case (case 4). Although the flux conversion for IMA counts is still under discussion, a quantitative estimate of the increase can be made from the

color contours in the bottom middle panel of Figure 3b. Assuming this 15 min sample in the mass-energy analysis contains the bulk of the escaping oxygen ions for the pass, there are at least ~10 times more present on this occasion compared to their counterparts in the other panels. The fact that the bulk of the ions are at low energies may be an artifact of the sampling, or it may be key to the physical process underlying their escape. Models of the pickup ion spatial distribution discussed above suggest a possible relationship between the low-altitude, lower energy ions and the higher-altitude more energetic ions. They also provide an explanation for the nonobservation of O^+ signatures for the three other events, related to the alteration of the pickup ion wake geometry by the enhanced ICME magnetic field and VEX orbital sampling. But a more detailed examination of this question requires further model development of the ICME-disturbed Venus interaction that is beyond the scope of the present report. We also expect an increase in the number of CME as solar activity rises to give us a picture of the responses of Venus picked up O^+ to much stronger (faster) events.

[30] **Acknowledgments.** Several of the authors (J.G.L., C.T.R., and D.A.B.) acknowledge support from the Venus Participating Scientist and Instrument Scientist Programs through NASA grants: NNG06GC61G (J.G.L.), NNG06GC62G (C.T.R.), NNX07AI62G S01 (D.A.B.). We are grateful to ESA and NASA for this opportunity to work with the Venus Express mission data.

References

Barabash, S., et al. (2006), The Analyzer of Space Plasmas and Energetic Atoms (ASPERA-3) for the Mars Express Mission, *Space Sci. Rev.*, *126*, 113–164, doi:10.1007/s11214-006-9124-8.

Barabash, S., et al. (2007a), The loss of ions from Venus through the plasma wake, *Nature*, *450*, 650–653, doi:10.1038/nature06434.

Barabash, S., et al. (2007b), The Analyser of Space Plasmas and Energetic Atoms (ASPERA-4) for the Venus Express mission, *Planet. Space Sci.*, *55*, 1772–1792, doi:10.1016/j.pss.2007.01.014.

Brace, L. H., W. T. Kasprzak, H. A. Taylor, R. F. Theis, C. T. Russell, A. Barnes, J. D. Mihalov, and D. M. Hunten (1987), The ionotail of Venus: Its configuration and evidence for ion escape, *J. Geophys. Res.*, *92*, 15–26, doi:10.1029/JA092iA01p00015.

Brace, L. H., R. E. Hartle, and R. F. Theis (1995), The nightward ion flow scenario at Venus revisited, *Adv. Space Res.*, *16*, 99–112, doi:10.1016/0273-1177(95)00255-D.

Carlsson, E., et al. (2006), Mass composition of the escaping plasma at Mars, *Icarus*, *182*, 320–328, doi:10.1016/j.icarus.2005.09.020.

Chassefiere, E. (1997), Loss of water on the young Venus: The effect of a strong primitive solar wind, *Icarus*, *126*, 229–232, doi:10.1006/icar.1997.5677.

Fedorov, A., et al. (2006), Structure of the Martian wake, *Icarus*, *182*, 329–336, doi:10.1016/j.icarus.2005.09.021.

Fox, J. L., and A. J. Kliore (1997), Ionosphere: Solar activity variations, in *Venus II*, edited by S. Bougher, D. L. Hunten, and R. Phillips, pp. 161–188, Univ. of Ariz. Press, Tucson.

Futaana, Y., S. Barabash, M. Yamauchi, R. Lundin, and S. McKenna-Lawlor (2007), Geo-effective solar flare events in December 2006: Space weather effect on Mars and Venus oxygen loss to space, *Eos Trans. AGU*, *88*(52), Fall Meet. Suppl., Abstract P23A-1087.

Grinspoon, D. H., and M. A. Bullock (2007), Searching for evidence of past oceans on Venus, paper presented at DPS Meeting 39, Am. Astron. Soc., Washington, D. C.

Jian, L., C. T. Russell, J. G. Luhmann, and R. M. Skoug (2006), Properties of interplanetary coronal mass ejections at one AU during 1995–2004, *Sol. Phys.*, *239*, 393–436, doi:10.1007/s11207-006-0133-2.

Jian, L., C. T. Russell, J. G. Luhmann, and R. M. Skoug (2008), Evolution of solar wind structures from 0.72 to 1 AU, *Adv. Space Res.*, *41*, 259–266, doi:10.1016/j.asr.2007.03.023.

Kallio, E., J. G. Luhmann, and J. G. Lyon (1998), Magnetic field near Venus: A comparison between Pioneer Venus Orbiter magnetic field observations and an MHD simulation, *J. Geophys. Res.*, *103*, 4723–4737, doi:10.1029/97JA02862.

Kallio, E., R. Jarvinen, and P. Janhunen (2006), Venus solar wind interaction: Asymmetries and the escape of O ions, *Planet. Space Sci.*, *54*, 1472–1481, doi:10.1016/j.pss.2006.04.030.

Kulikov, Y. N., et al. (2006), Atmospheric and water loss from early Venus, *Planet. Space Sci.*, *54*, 1425–1444, doi:10.1016/j.pss.2006.04.021.

Lammer, H., et al. (2006), Loss of hydrogen and oxygen from the upper atmosphere of Venus, *Planet. Space Sci.*, *54*, 1445–1456, doi:10.1016/j.pss.2006.04.022.

Lindsay, G. M., C. T. Russell, and J. G. Luhmann (1995), Coronal mass ejection and stream interaction region characteristics and their potential geomagnetic effectiveness, *J. Geophys. Res.*, *100*, 16,999–17,014, doi:10.1029/95JA00525.

Luhmann, J. G., and T. E. Cravens (1991), Magnetic fields in the ionosphere of Venus, *Space Sci. Rev.*, *55*, 201–274, doi:10.1007/BF00177138.

Luhmann, J. G., and J. U. Kozyra (1991), Dayside pickup oxygen ion precipitation at Venus and Mars–Spatial distributions, energy deposition and consequences, *J. Geophys. Res.*, *96*, 5457–5467, doi:10.1029/90JA01753.

Luhmann, J. G., S. A. Ledvina, J. G. Lyon, and C. T. Russell (2006), Venus O+ pickup ions: Collected PVO results and expectations for Venus Express, *Planet. Space Sci.*, *54*, 1457–1471, doi:10.1016/j.pss.2005.10.009.

Luhmann, J. G., W. T. Kasprzak, and C. T. Russell (2007), Space weather at Venus and its potential consequences for atmosphere evolution, *J. Geophys. Res.*, *112*, E04S10, doi:10.1029/2006JE002820.

Mihalov, J. D., and A. Barnes (1982), The distant interplanetary wake of Venus- Plasma observations from Pioneer Venus, *J. Geophys. Res.*, *87*, 9045–9053, doi:10.1029/JA087iA11p09045.

Mihalov, J. D., C. T. Russell, W. T. Kasprzak, and W. C. Knudsen (1995), Observations of ionospheric escape on Venus' nightside, *J. Geophys. Res.*, *100*, 19,579–19,584, doi:10.1029/95JA01342.

Miller, K. L., and R. C. Whitten (1991), Ion dynamics in the Venus ionosphere, *Space Sci. Rev.*, *55*, 165–200, doi:10.1007/BF00177137.

Moore, K. R., D. J. McComas, C. T. Russell, and J. D. Mihalov (1990), A statistical study of ions and magnetic fields in the Venus magnetotail, *J. Geophys. Res.*, *95*, 12,005–12,018, doi:10.1029/JA095iA08p12005.

Moore, K. R., D. J. McComas, C. T. Russell, S. S. Stahara, and J. R. Spreiter (1991), Gasdynamic modeling of the Venus magnetotail, *J. Geophys. Res.*, *96*, 5667–5681, doi:10.1029/90JA02251.

Mulligan, T., C. T. Russell, and J. G. Luhmann (1998), Solar cycle evolution of the structure of magnetic clouds in the inner heliosphere, *Geophys. Res. Lett.*, *25*, 2959–2962, doi:10.1029/98GL01302.

Phillips, J. L., J. G. Luhmann, W. C. Knudsen, and L. H. Brace (1988), Asymmetries in the location of the Venus ionopause, *J. Geophys. Res.*, *93*, 3927–3941, doi:10.1029/JA093iA05p03927.

Svedhem, H., et al. (2007), Venus Express-The first European mission to Venus, *Planet. Space Sci.*, *55*, 1636–1652, doi:10.1016/j.pss.2007.01.013.

Terada, N., S. Machida, and H. Shinagawa (2002), Global hybrid simulation of the Kelvin-Helmholtz instability at the Venus ionopause, *J. Geophys. Res.*, *107*(A12), 1471,doi:10.1029/2001JA009224.

Vaisberg, O. L., et al. (1995), Ion populations in the tail of Venus, *Adv. Space Res.*, *16*, 105–118, doi:10.1016/0273-1177(95)00217-3.

Zhang, T. L., et al. (2006), Magnetic field investigation of the Venus plasma environment: Expected new results from Venus Express, *Planet. Space Sci.*, *54*, 1336–1343, doi:10.1016/j.pss.2006.04.018.

S. Barabash, E. Carlsson, and Y. Futaana, Swedish Institute of Space Physics, Box 812, SE-981, 28 Kiruna, Sweden. (stas@irf.se; ella@irf.se; futaana@irf.se)

D. A. Brain, S. A. Ledvina, and J. G. Luhmann, Space Sciences Laboratory, University of California, 7 Gauss Way, Berkeley, CA 94720-7450, USA. (brain@ssl.berkeley.edu; ledvina@ssl.berkeley.edu; jgluhman@ssl.berkeley.edu)

A. Fedorov, Centre d'Etude Spatiale des Rayonnements, BP-4346, F-31028 Toulouse CEDEX 4, France. (andrei.fedorov@cesr.fr)

J. G. Lyon, Department of Physics and Astronomy, Dartmouth College, 6127 Wilder Laboratory, Hanover, NH 03755-3528, USA. (john.lyon@dartmouth.edu)

C. T. Russell, Institute of Geophysics and Planetary Physics, University of California, Box 951567, Los Angeles, CA 90095, USA. (ctrussel@igpp.ucla.edu)

T. L. Zhang, Space Research Institute, Austrian Academy of Sciences, 8042 Graz, Austria. (tielong.zhang@oeaw.ac.at)